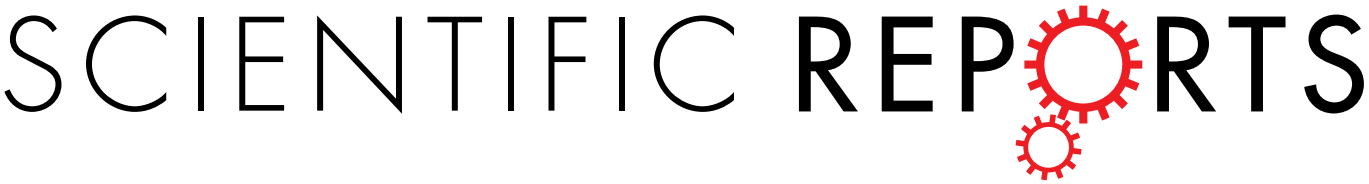

OPEN

Diamond formation in the deep lower mantle: a high-pressure reaction of $MgCO_3$ and SiO_2

Received: 30 August 2016
Accepted: 07 December 2016
Published: 13 January 2017

Fumiya Maeda[1], Eiji Ohtani[1,2], Seiji Kamada[1,3], Tatsuya Sakamaki[1], Naohisa Hirao[4] & Yasuo Ohishi[4]

Diamond is an evidence for carbon existing in the deep Earth. Some diamonds are considered to have originated at various depth ranges from the mantle transition zone to the lower mantle. These diamonds are expected to carry significant information about the deep Earth. Here, we determined the phase relations in the $MgCO_3$-SiO_2 system up to 152 GPa and 3,100 K using a double sided laser-heated diamond anvil cell combined with *in situ* synchrotron X-ray diffraction. $MgCO_3$ transforms from magnesite to the high-pressure polymorph of $MgCO_3$, phase II, above 80 GPa. A reaction between $MgCO_3$ phase II and SiO_2 ($CaCl_2$-type SiO_2 or seifertite) to form diamond and $MgSiO_3$ (bridgmanite or post-perovsktite) was identified in the deep lower mantle conditions. These observations suggested that the reaction of the $MgCO_3$ phase II with SiO_2 causes formation of super-deep diamond in cold slabs descending into the deep lower mantle.

Carbon is circulated around the surface and interior of the Earth with subducting slabs and volcanic eruptions; subduction carries carbon-bearing rocks to the Earth's interior and volcanic eruption expels carbon-bearing gas, lavas and rocks from the interior of the Earth[1]. The flux of subducted carbon within oceanic plates is estimated to be more than 5 Tmol/yr, almost twice as large as the expelled-carbon flux, 2–3 Tmol/yr, through arc magmatism[2]. This difference suggests the existence of carbon reservoirs in the deep Earth[1,2].

One source of direct evidence for deep carbon is carbon-bearing samples originating from the Earth's interior. Diamond is evidence of quite a deeper-origin carbon. In particular, some diamonds, called 'super-deep diamond', are thought to arise from the mantle transition zone or the lower mantle[3–8]. The inclusions in super-deep diamond may supply information on the lithology, water content, and/or elemental distribution in deep parts of the Earth[3–8].

Subducting slabs play a key role for carrying carbon-bearing phases into the deep Earth and forming super-deep diamond[3–5]. Altered rocks in the oceanic crust contains the large amount of carbon such as organic carbon or carbonate minerals, which can be the deep reservoir of subducted carbon[9,10]. These carbonate minerals or melts may change to diamond if they become unstable in the Earth during the subduction process[3,5,11–13]. The stability of carbonates has been investigated using high-pressure experiments and *ab initio* calculations, and $MgCO_3$ magnesite is determined to be stable under the high-pressure and high-temperature conditions expected during subduction[11–20]. The existence of carbonate (or carbonatite melt) in the deep mantle is supported by the discovery of carbonate as inclusions in diamonds originating from the mantle transition zone and/or the lower mantle[3,5].

Since SiO_2 is one of the abundant components and also is an important phase in deeply subducted slabs[21–23], the $MgCO_3$-SiO_2 system may be applied to the slabs descending into the lower mantle. SiO_2 phases may change to its high-pressure polymorph, such as coesite, stishovite, $CaCl_2$-type phase and seifertite[24,25]. Magnesite is expected to break down to CO_2 or diamond by reacting with silica minerals in the $MgCO_3$-SiO_2 system in subducting process[12,13,26,27] although the detail of its phase relation has not yet been clarified. Knowledge of the reactions in this system at high pressure and high temperature may provide important insights into the carbon-related processes in the deep mantle, such as the origin of super-deep diamond and melting or oxidation by release of

[1]Department of Earth Science, Graduate School of Science, Tohoku University, Sendai, 980-8578, Japan. [2]V.S. Sobolev Institute of Geology and Mineralogy, SB RAS, Novosibirsk, 630090, Russia. [3]Frontier Research Institute for Interdisciplinary Sciences, Tohoku University, Sendai, 980-8578, Japan. [4]Japan Synchrotron Radiation Research Institute, Sayo, Hyogo 679-5198, Japan. Correspondence and requests for materials should be addressed to F.M. (email: f.maeda@dc.tohoku.ac.jp)

volatile components[13,28]. We used a laser-heated diamond anvil cell (LHDAC) combined with a high-pressure and high-temperature *in situ* synchrotron X-ray diffraction (XRD) technique to quantify the phase relations of the $MgCO_3$-SiO_2 system down to the lowermost-mantle conditions. Our objective is to clarify the behavior of carbon in the lower mantle and to model the origin of super-deep diamond.

Results

We observed the phase relation of $MgCO_3$ and SiO_2 system up to 152 GPa and 3,100 K (see Supplementary Table s S1 and S3). Diamond and bridgmanite may be formed through the following reactions[12,13,28]:

$$SiO_2 + MgCO_3 \rightarrow MgSiO_3 + CO_2. \quad (1)$$

$$CO_2 \rightarrow C + O_2. \quad (2)$$

Or, the following reaction is also possible:

$$SiO_2 + MgCO_3 \rightarrow MgSiO_3 + C + O_2. \quad (3)$$

Bridgmanite and diamond were observed using XRD, in a run product recovered from 83 GPa and 1,780 K (Fig. 1a). The X-ray pattern was taken at an ambient condition without DAC, of which surface showed no damage after the experiments. The high-pressure phase of CO_2 was not detected in most runs, matching the previous studies on the $MgCO_3$-SiO_2 system[12,13]. We successfully detected the high-pressure phase of CO_2, CO_2-VI[29] in one run made by *in situ* X-ray diffraction at 83 GPa and 1,780 K (see Supplementary Table S1). Thus, occurrence of reactions (1) and (2) or (3) were thus confirmed.

The structures of the $MgCO_3$ high-pressure phases and their phase transition boundary are controversial and the data on their compression behaviors are very limited. A recent *ab initio* study reported a monoclinic post-magnesite phase, $MgCO_3$ phase II (C2/m) at 300 K and pressures from 82 to 138 GPa[16]. On the other hand, the latest study reported the stabilization of another post-magnesite phase, having space group P-1, at 300 K and 85–101 GPa, which transforms to $MgCO_3$ phase II (C2/m) at 101 GPa and 300 K[19]. We conducted an *in situ* XRD study of $MgCO_3$ using a double sided laser-heated diamond anvil cell in the pressure range from 85 GPa to 132 GPa at about 2,500–3,000 K. Diffraction peaks after heating corresponded to the $MgCO_3$ phase II[16] in the same pressure range (see Supplementary Fig. S1 and Supplementary Table S2). The volumes of $MgCO_3$ phase II in each run were estimated by fitting XRD patterns (see Supplementary Table S2). We then fitted the estimated volumes using the second order Birch-Murnaghan equations of state (BMEOS). As a result, the unit-cell volume at ambient condition (V_0) and isothermal bulk modulus ($K_{300K,\,0}$) of magnesite phase II were estimated to be 498.9(5) Å^3 and 154.9(7) GPa, respectively (K' = 4; fixed). These values are consistent with the V_0 and K_{T0} calculated by ref. 16, $V_0 = 503.36$ Å^3 (Z = 12) and $K_0 = 156.76$ GPa using the third order BMEOS (K' = 4.12).

$MgCO_3$ phase II was identified in $MgCO_3$-SiO_2 system at pressures above 100 GPa by comparing the XRD patterns of the runs in the $MgCO_3$-SiO_2 system with the results of $MgCO_3$ compression (see Supplementary Inf ormation Table S2). This enabled us to distinguish the $MgSiO_3$ bridgmanite/post-perovskite phase from $MgCO_3$ phase II in the XRD patterns (Fig. 1b). The $MgSiO_3$ post-perovskite phase is thought to be formed by either reaction (1) or (3), where $MgCO_3$ and SiO_2 are considered to be $MgCO_3$ phase II and seifertite, respectively. XRD spots (111) indicating diamond were also observed in some runs conducted at pressures greater than 100 GPa (see Supplementary Fig. S2). The number of diamond spots was limited and their intensities were weak. They did not appear in all 1D XRD patterns at high pressure. However, diamond created in high-pressure and high-temperature conditions was confirmed in the recovered run products (Fig. 1a and c).

Figure 2 shows the phase diagram of the $MgCO_3$-SiO_2 system based on the present and previous studies. The temperature of magnesite decarbonation is consistent with ref. 13 but higher than ref. 12 up to 70 GPa. We discovered the phase transformations from $CaCl_2$-type SiO_2 + $MgCO_3$ phase II to bridgmanite + diamond + O_2 and from seifertite + $MgCO_3$ phase II to bridgmanite/post-perovskite + diamond + O_2 for the first time in this experiment. The decomposition boundary of CO_2 has a steep gradient in the present phase diagram of $MgCO_3$-SiO_2 system which is not consistent with the results of any previous studies on CO_2, such as decomposition[28] or phase transition of CO_2[30].

Discussion

Since the reactions between $MgCO_3$ and SiO_2 may be expected in deeply subducted slabs[13,26,27], we should consider the phase relations in the $MgCO_3$-SiO_2 system on subducting depth-temperature paths. The phase boundaries of the $MgCO_3$-SiO_2 system are shown with several slab geotherms[31] in Fig. 3. The slab geotherms in Fig. 3a are models based on the geological observations[32] and mineralogical hypothesis[31] in the present Earth. The super-deep diamonds form Juina kimberlite were considered to be related to Gondwana subduction and formed at 150 Ma[5]. Therefore, the colder geotherms like the modern Earth may be useful to be compared with the $MgCO_3$-SiO_2 reactions. The reactions in this system provide important information for understanding the stability limits of $MgCO_3$ in deep subduction.

The reaction between $MgCO_3$ and SiO_2 may not occur down to the top of the lower mantle but can occur at depths from 1,000 to 2,000 km in various subducting slabs. In "hot" and "cold" slabs[31], which are comparable to Mexico and the various Pacific subduction paths respectively[32], magnesite can react with stishovite to form bridgmanite and CO_2 at depths of around 1,700 km, and subsequently CO_2 can decompose to diamond and O_2 at the greater depths. Therefore, super-deep diamond could be formed at depths greater than 1,700 km in cold slabs.

The path of "very cold" slabs[31] such as Tonga subduction[32] may pass through the 'bottleneck' region in the phase diagram at ~80 GPa corresponding to the depth near the $MgCO_3$ magnesite-phase II boundary (~1,900 km). $MgCO_3$

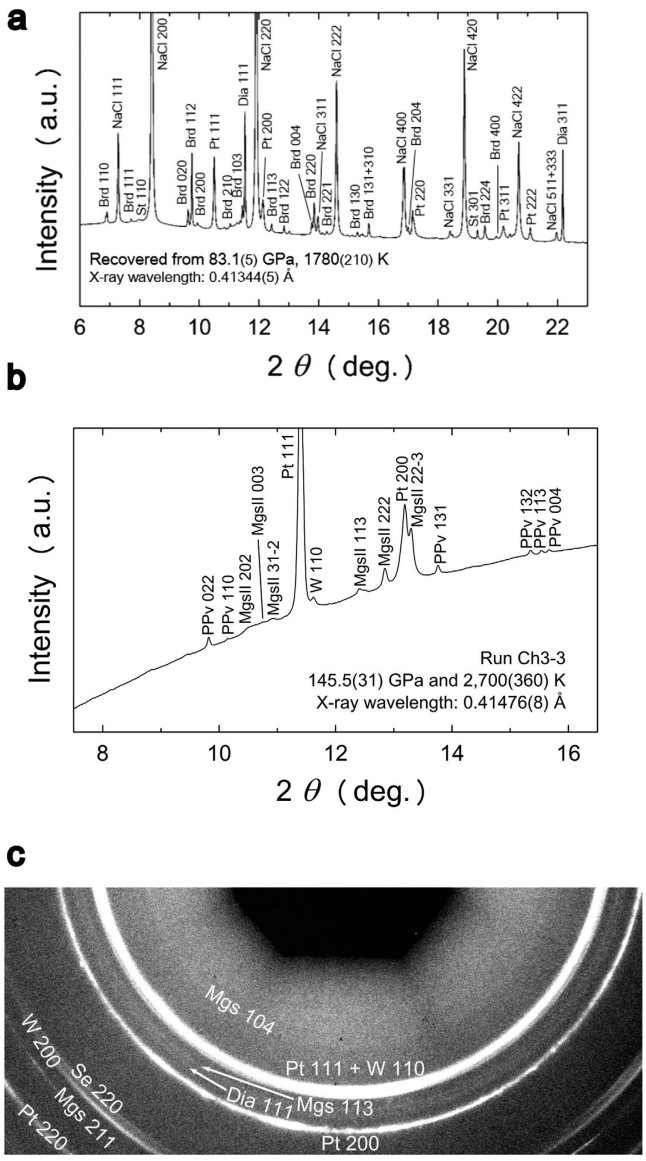

Figure 1. XRD patterns of the reaction products in the $MgCO_3$-SiO_2 system. (**a**) XRD patterns obtained under the ambient condition for the samples recovered from 83.1(5) GPa and 1,780(210) K. The X-ray pattern was taken at ambient condition without DAC, of which surface showed no damage after the experiment. The abbreviations represent as follow: St: stishovite, Brd: bridgmanite, Dia: diamond, Pt: platinum, W: tungsten (gasket), NaCl: sodium chloride (pressure medium). (**b**) *In situ* XRD patterns obtained at 145.5 (31) GPa and 2,700 (360) K. (**c**) 2D XRD images of a sample recovered from 145.5 (31) GPa and 2,700 (360) K obtained at ambient condition without DAC. The abbreviations represent as follow: Se: seifertite, Mgs: magnesite, MgsII: $MgCO_3$ phase II, PPv: $MgSiO_3$ post-perovskite phase, Dia: diamond, Pt: platinum, W: tungsten (gasket).

in such slabs may descend to the base of the lower mantle because the stability field of $MgSiO_3$ + diamond + O_2 is relatively narrow or absent in the pressure-temperature path of very cold slabs (Fig. 3a). If $MgCO_3$ is able to survive beyond 1,900-km depth, $MgCO_3$ phase II will be formed and subsequently decompose to $MgSiO_3$ post-perovskite phase + diamond + O_2 by a reaction with seifertite at the base of the lower mantle due to heating from the outer core.

Slabs in the early Earth, Archean/Proterozoic age, might descend into the hotter mantle than the modern adiabat[33]. The hotter subduction could restrict the $MgCO_3$ subduction into the deep lower mantle because of the reaction (1) in the shallower mantle (Fig. 3). In this case, CO_2 might be a significant carbon carrier in the subducted slabs although its stability has been still controversial under high pressure and high temperature conditions[28,30]. If early slab temperatures had been higher than the modern mantle adiabat[33], the formation of CO_2 fluid[28] or melting in the $MgCO_3$-SiO_2 system[26] would be expected down to the mantle transition zone. These phenomena might prevent the subduction of carbon-bearing phases into the lower mantle. This might be the reason why the reports of the old super-deep diamonds are absent.

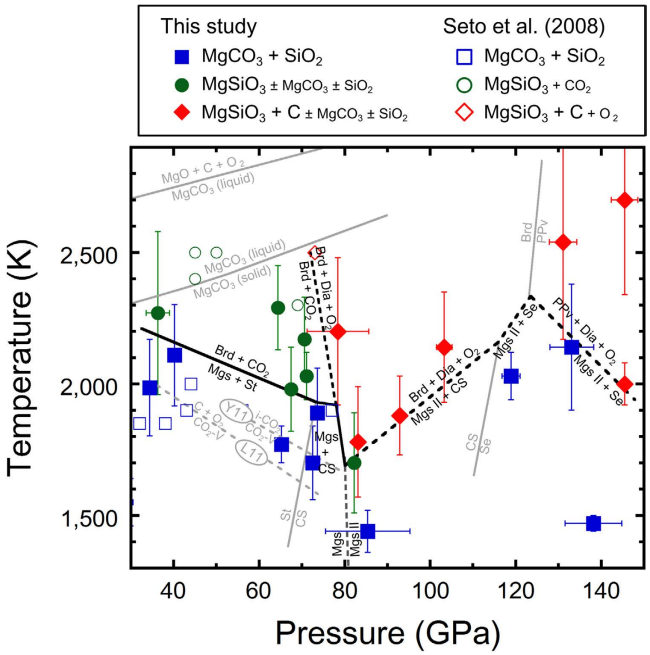

Figure 2. Phase diagram of the $MgCO_3$-SiO_2 system. The closed and open symbols represent the results of the present study and ref. 13, respectively. The colors of the symbols show the observed phases as follow: blue: $MgCO_3 + SiO_2$, green: $MgSiO_3 \pm MgCO_3 \pm SiO_2$ ($+CO_2$), red: $MgSiO_3 + C \pm MgCO_3 \pm SiO_2$. The present phase boundaries in the $MgCO_3$-SiO_2 system are shown by black solid and dotted lines. The non-equilibrium phases are shown as a small font in the index column above the phase diagram. The referred phase boundaries between CO_2-V and ionic CO_2[30] and between CO_2-V and $C + O_2$[28] are gray dotted lines, shown by 'Y11' and 'L11', respectively. The phase boundaries of SiO_2 stishovite (St)-to-$CaCl_2$-type SiO_2 (CS)[24] and $CaCl_2$-type SiO_2 (CS)-to-seifertite (Se)[25], the phase boundary of $MgSiO_3$ bridgmanite (Br)-to-post-perovskite phase (PPv)[37], and those of $MgCO_3$ magnesite-to-$MgCO_3$ liquid and $MgCO_3$ liquid-to-$MgO + CO_2$[20] are shown by gray solid lines.

The reaction in the "very cold" slab may play an important role in formation of super-deep diamond in the deep lower mantle. Reference 5 summarized the mineral inclusions in diamond, and estimated the formation depths of diamonds in the mantle. Some diamonds from São Luiz, Juina province, Brazil have inclusions of orthopyroxene which are a psuedomorph of bridgmanite and TAPP (tetragonal almandine-pyrope phase) suggesting the top of the lower mantle, 660–750 km depths. They also suggested that some diamonds with inclusions of aluminous bridgmanite pseudomorph from the same locality, Juina, Brazil, might be originated at the depths greater than 750 km, although the exact depth limit was not estimated. On the other hand, Diamonds containing the iron-rich (Mg,Fe)O inclusions[6,8] were considered to be originated from the deep lower mantle (1,700–2,900 km) because of iron enrichment by the spin transition at depths greater than about 1,700 km[34–36], or by the phase transition from bridgmanite to post perovskite at around 2,700-km depth[37–41], although it is a debated matter whether iron-rich (Mg,Fe)O inclusions are the signature of the bottom of the lower mantle or not.

The mechanism of diamond formation discovered here may explain the origin of super-deep diamond from the deep lower mantle such as those reported from the limited locality in Brazil[5,6,8]. Although we did not consider the effects of fO_2[42,43] in the reaction (3) because of the technical difficulty for controlling fO_2 in the DAC experiments, we can expect the above reaction in the presence of iron in the average lower mantle with the fO_2 condition below the iron-wüstite buffer[44]. When metallic iron exists in the system, iron oxide can be formed by the reaction with O_2 in the run products. The role of iron is also important in formation of high-pressure polymorphs of carbonate[18,45,46]. The latest studies reported that the iron-magnesium carbonate transforms into the several new phases: $Fe_4(CO_4)_3$ phase having unknown structure[18], orthorhombic (Mg,Fe)CO_3 phase II[45], or the unquenchable phases with unexpected stoichiometry ($Mg_2Fe_2(C_4O_{13}) + Fe_{13}O_{19}$) that coexist under the lower mantle[46]. Therefore, we may need to modify the present phase relation further in the iron bearing system. However, we can consider that the reaction of diamond formation could also occur in the iron-bearing system since iron oxides and/or FeO-bearing bridgmanite and ferropericlase can be formed in deep subducted slabs.

Released oxygen will oxidize the ferrous iron in mantle minerals or the metallic iron penetrated from the outer core at the core-mantle boundary[28,47]. The oxidation of metallic iron can generate FeO. As a result, the iron-rich magnesiowüstite of (Mg,Fe)O[6,8] would be formed as inclusions in the deepest diamonds, although it is not a single process for generation of FeO enrichment in magnesiowustite as inclusions in diamond and other processes of the redox change in the shallower depths could also have generated similar iron enrichment. Future studies are needed to elucidate the ultra-deep iron-carbon redox coupling processes and their influence on formation of super-deep diamond.

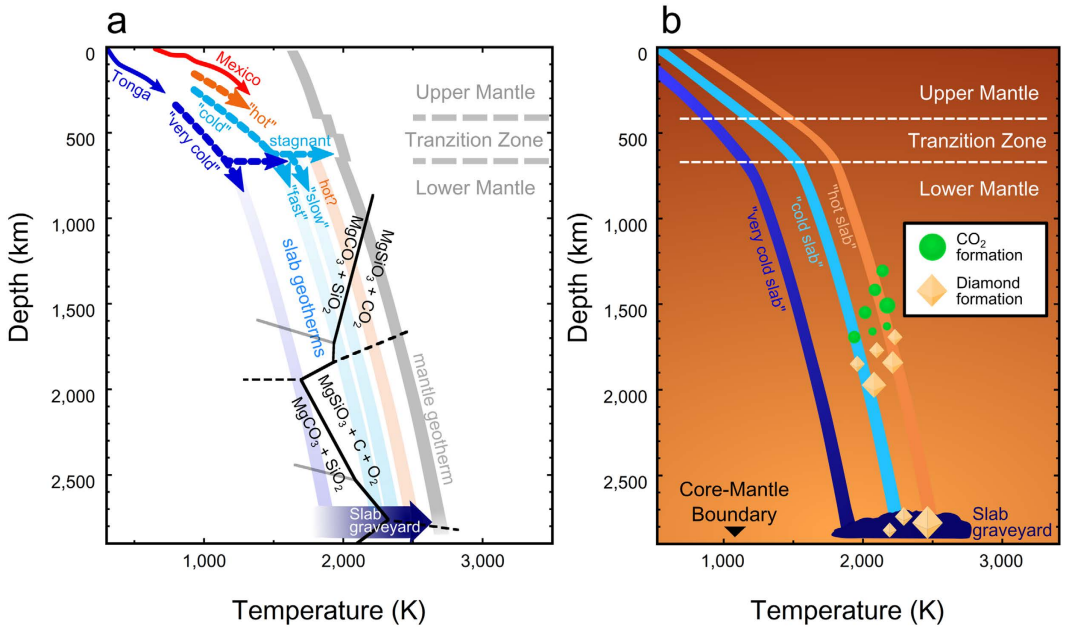

Figure 3. Change of carbon-bearing phases in the slabs descending into the lower mantle. (**a**) The phase boundaries in the $MgCO_3$-SiO_2 system are denoted with the Earth's geotherms. The gray solid zone shows the mantle adiabat[33]. The blue and red solid arrows are the depth-temperature paths of Tonga and Mexico subduction zones, where the coldest and hottest slabs were modeled in ref. 32, respectively. The hypothetical models of the "hot", "cold" and "very cold" slabs[31] are shown by the orange, light blue and blue arrows, respectively, and the zone of each color is extrapolation of each path. The series of paths of cold-slab geotherm below the mantle transition zone represent the case of the fast subduction, stagnant and the slow subduction[31]. (**b**) The schematic model of the super-deep diamond's formation. The orange, light blue and blue lines represent the "hot", "cold" and "very cold" subducting slabs[31], respectively. The green circles and diamond-shaped symbols indicate the possible depth of CO_2 and diamond formation, respectively.

Methods

A natural single crystal of magnesite (Bahia, Brazil, $Mg_{0.994}Ca_{0.003}Fe_{0.003}CO_3$) and a reagent quartz (reagent grade, Woko) were ground to fine powders in an agate mortar for 1 hour. The powders were mixed 1:1 by mole fraction and ground in an agate mortar for 30 min to homogenize the mixture. High-pressure and high-temperature experiments were conducted using a double sided LHDAC. The culet diameters of the diamond anvils were between 100 and 350 μm. The sample chamber drilled in rhenium or tungsten gaskets ranges from 30 to 100 μm in diameter and from 40 to 80 μm in the thickness depending on the culet sizes. NaCl or SiO_2 glass was used as the pressure medium and thermal insulator.

Platinum was included in the sample chamber as a laser absorber. We used three sample configurations to obtain stable temperatures at high pressures: Run Ch1-3-layer-chamber, Run Ch2-5-layer-chamber and Run Ch3-Pt/W-doughnut-chamber (Supplementary Table 1). In Run Ch1, 5 wt. % platinum powder (platinum black, purity 99.9%, Mitsuwa Chemicals) was mixed with magnesite and quartz starting material (Ch1) and this was sandwiched by a pressure medium. On the other hand, in Run Ch2, the magnesite and quartz mixture was sandwiched by platinum foils (purity 99.9%, Nilaco). Run Ch2 aimed to reduce the temperature gradient at the heating spot during double-sided laser heating.

The samples were heated by double-sided fiber lasers (SPI LASER) of wavelength 1.090 μm at Tohoku University in Sendai, Japan and 1.070 μm at BL10XU of SPring-8 in Hyogo, Japan. The heating duration was 10–120 minutes. Temperature was determined by fitting the emission spectra from the heated samples to the gray-body radiation formula.

In situ synchrotron X-ray diffraction (XRD) was conducted to identify the experimental products. We acquired the XRD patterns of the samples at high pressure up to 152 GPa in the temperature range from 300 K to 3,100 K at BL10XU of SPring-8. The collimator was 20 μm in diameter and the typical wavelength of X-ray was 0.41414(9) Å. An imaging plate (Rigaku, R-AXIS IV^{++}) and a charge coupled device (Bruker, AXS SMART APEX) detectors were used for acquiring the XRD patterns. The pressures of *in situ* experiments were determined based on the equation of state of Pt[48]. Thermal pressure was estimated based on Mie–Grüneisen–Debye model[49,50]. In Runs Ch3-1 and Ch2-5, the sample was heated at Tohoku University and observed after temperature quenching at high pressure using XRD at BL10XU of SPring-8. In Ch3-1, the sample was recovered to the ambient condition at Tohoku University after the temperature quenching and pressure determination using ruby fluorescence method[51]. Since thermal pressure could not be estimated in Runs Ch3-1 and Ch2-5, we considered the pressure errors up to ±10 GPa for pressures at high temperature during laser heating. This is almost equivalent to the maximum pressure increase by laser heating in the *in situ* XRD experiments.

The high-pressure phase transition of $MgCO_3$ was confirmed in two series of runs, Ms-1 and Ms-2 in addition to the $MgCO_3$-SiO_2 system (Supplementary Table 2). These runs were conducted using a membrane-type diamond anvil cell. The natural magnesite and Pt powder were sandwiched by the same magnesite in the sample chamber. Pt powder was used as a pressure maker and laser absorber. Magnesite was compressed to about 100 GPa, and then pre-heated to temperature of less than 1,500 K using CO_2 laser at Tohoku University in order to crystallize the compressed sample in Run Ms-1. We conducted laser heating at 2,500–3,000 K for 5–20 min in order to obtain the obvious XRD patterns of the $MgCO_3$ high-pressure phase using SPI fiber laser in two series of runs, Ms-1 and Ms-2. XRD patterns were acquired at high pressure and 300 K after quenching.

Temperatures in some experiments increased suddenly to above 3,000 K in the Runs Ch1-1, Ch1-2, Ch1-3 and Ch 2-1 using platinum as a laser absorber (Supplementary Table 1). This phenomenon may correspond to the 'temperature jump' reported by ref. 13. The sudden temperature increase was also observed at high pressures and above 2,000 K when a Pt powder (Run Ch1) and Pt foil (Run Ch2) was used as the laser absorber. These results indicate that large temperature fluctuation may be caused by the volume change following reactions, phase transitions and/or melting of the sample.

References

1. Dasgupta, R. & Hirschmann, M. M. The deep carbon cycle and melting in the Earth's interior. *Earth Planet. Sci. Lett.* **298,** 1–13 (2010).
2. Kerrick, D. C. & Connolly, J. A. D. Metamorphic devolatilization of subducted marine sediments and the transport of volatiles into the Earth's mantle. *Nature* **411,** 293–296 (2001).
3. Brenker, F. E. *et al.* Carbonates from the lower part of transition zone or even the lower mantle. *Earth Planet. Sci. Lett.* **260,** 1–9 (2007).
4. Harte, B. Diamond formation in the deep mantle: the record of mineral inclusions and their distribution in relation to mantle dehydration zones. *Mineral. Mag.* **74,** 189–215 (2010).
5. Harte, B. & Richardson, S. Mineral inclusions in diamonds track the evolution of a Mesozoic subducted slab beneath West Gondwanaland. *Gond. Res.* **21,** 236–245 (2012).
6. Hayman, P., Kopylova, M. & Kaminsky, F. Lower mantle diamonds from Rio Soriso (Juina area, Mato Grosso, Brazil). *Contrib. Mneral. Petrol.* **149,** 430–445 (2005).
7. Pearson, D. G. *et al.* Hydrous mantle transition zone indicated by ringwoodite included within diamond. *Nature* **507,** 221–224 (2014).
8. Wirth, R., Dobrzhinetskaya, L., Harte, B., Schreiber, A. & Green, H. W. High-Fe (Mg, Fe)O inclusion in diamond apparently from the lowermost mantle. *Earth Planet. Sci. Lett.* **404,** 365–375 (2014).
9. Plank, T. & Langmuir, C. H. The chemical composition of subducting sediment and its consequences for the crust and mantle. *Chem. Geol.* **145,** 325–394 (1998).
10. Alt, J. C. & Teagle, D. A. H. The uptake of carbon during alteration of ocean crust. *Geochem. Cosmochim. Acta* **63,** 1527–1535 (1999).
11. Biellmann, C., Gillet, P., Guyot, F., Peyronneau, J. & Reynard, B. Experimental evidence for carbonate stability in the Earth's lower mantle. *Earth Planet. Sci. Lett.* **118,** 31–41 (1993).
12. Takafuji, N., Fujino, K., Nagai, T., Seto, Y. & Hamane, D. Decarbonation reaction of magnesite in subducting slabs at the lower mantle. *Phys. Chem. Miner.* **33,** 651–654 (2006).
13. Seto, Y., Hamane, D., Nagai, T. & Fujino, K. Fate of carbonates within oceanic plates subducted to the lower mantle, and a possible mechanism of diamond formation. *Phys. Chem. Miner.* **35,** 223–229 (2008).
14. Fiquet, G. *et al.* Structural refinements of magnesite at very high pressure. *Am. Mineral.* **87,** 1261–1265 (2002).
15. Isshiki, M. *et al.* Stability of magnesite and its high-pressure form in the lowermost mantle. *Nature* **427,** 60–62 (2004).
16. Oganov, A. R., Ono, S., Ma, Y., Glass, C. W. & Garcia, A. Novel high-pressure structures of $MgCO_3$, 176 $CaCO_3$ and CO_2 and their role in Earth's lower mantle. *Earth Planet. Sci. Lett.* **273,** 38–47 (2008).
17. Boulard, E. *et al.* New host for carbon in the deep Earth. *Proc. Natl. Acad. Sci. USA* **108,** 5184–5187 (2011).
18. Boulard, E. *et al.* Experimental investigation of the stability of Fe-rich carbonates in the lower mantle. *J. Geophys. Res.* **117,** B02208 (2012).
19. Pickard, C. J. & Needs, R. J. Structures and stability of calcium and magnesium carbonates at mantle pressures. *Phys. Rev. B* **91,** 104101 (2015).
20. Solopova, N. A., Dubrovinsky, L., Spivak, A. V., Litvin, Y. A. & Dubrovinskaia, N. Melting and decomposition of $MgCO_3$ at pressures up to 84 GPa. *Phys. Chem. Miner.* **42,** 73–81 (2015).
21. Ishii, T., Kojitani, H. & Akaogi, M. High-pressure phase transitions and subduction behavior of continental crust at pressure–temperature conditions up to the upperpart of the lower mantle. *Earth Planet. Sci. Lett.* **357–358,** 31–41 (2012).
22. Ono, S. Stability limits of hydrous minerals in sediment and mid-ocean ridge basalt compositions: Implications for water transport in subduction zones. *J. Geophys. Res.* **103,** 18253–18267 (1998).
23. Ricolleau, A. *et al.* Phase relations and equation of state of a natural MORB: Imprication for the density profile of subducted oceanic crust in the Earth's lower mantle. *J. Geophys. Res.* **115,** B08202 (2010).
24. Murakami, M., Hirose, K., Ono, S. & Ohishi, Y. Stability of $CaCl_2$-type and PbO_2-type SiO_2 at high pressure and temperature determined by *in-situ* X-ray measurements. *Geophys. Res. Lett.* **30,** 1207 (2003).
25. Grocholski, B., Shim, S.-H. & Prakapenka, V. B. Stability, metastability, and elastic properties of a dense silica polymorph, seifertite. *J. Geophys. Res.: Solid Earth* **118,** 4745–4757 (2013).
26. Litasov, K. D., Fei, Y., Ohtani, E., Kuribayashi, T. & Fumakoshi, K. Thermal equation of state of magnesite to 32 GPa and 2073 K. *Phys. Earth Planet. Inter.* **168,** 191–203 (2008).
27. Kakizawa, S., Inoue, T., Suenami, H. & Kikegawa, T. Decarbonation and melting in $MgCO_3$-SiO_2 system at high temperature and high pressure. *J. Mineral. Petrol. Sci.* **110,** 179–188 (2015).
28. Litasov, K. D., Goncharov, A. F. & Hemley, R. J. Crossover from melting to dissociation of CO_2 under pressure: Implications for the lower mantle. *Earth Planet. Sci. Lett.* **309,** 318–323 (2011).
29. Iota, V. *et al.* Six-fold coordinated carbon dioxide VI. *Nature Matt.* **6,** 34–38 (2007).
30. Yoo, C.-S., Sengupta, A. & Kim, M. Carbon dioxide carbonates in the Earth's mantle: implications to the deep carbon cycle. *Angew. Chem.* **125,** 11415–11418 (2011).
31. Komabayashi, T., Omori, S. & Maruyama, S. Petrogenetic grid in the system MgO-SiO_2-H_2O up to 30 GPa, 1600 °C: applications to hydrous peridotite subducting into the Earth's deep interior. *J. Geophys. Res.* **109,** B03206 (2004).
32. Syracuse, E. M., van Keken, P. E. & Abers, G. A. The global range of subduction zone thermal models. *Earth Planet. Sci. Lett.* **183,** 73–90 (2010).
33. Katsura, T., Yoneda, A., Yamazaki, D., Yoshino, T. & Ito, E. Adiabatic temperature profile in the mantle. *Phys. Earth Planet. Inter.* **183,** 212–218 (2010).
34. Badro, J. *et al.* Iron partitioning in Earth's mantle: toward a lower mantle discontinuity. *Science* **300,** 789–791 (2003).

35. Speziale, S. *et al.* Iron spin transition in Earth's mantle. *Proc. Natl. Acad. Sci.* **102,** 17918–17922 (2005).
36. Lin, J.-F. *et al.* Pressure-induced electronic spin transition of iron in magnesiowustite-(Mg,Fe)O. *Phys. Rev. B* **73,** 113107 (2006).
37. Komabayashi, T. *et al.* Simultaneous volume measurements of post-perovskite and perovskite in $MgSiO_3$ and their thermal equations of state. *Earth Planet. Sci. Lett.* **265,** 515–524 (2008).
38. Murakami, M., Hirose, K., Kawamura, K., Sata, N. & Ohishi, Y. Post-perovskite phase transition in $MgSiO_3$. *Science* **304,** 855–858 (2004).
39. Murakami, M., Hirose, K., Sata, N. & Ohishi, Y. Post-perovskite phase transition and mineral chemistry in the pyrolytic lowermost mantle. *Geophys. Res. Lett.* **32,** L03304 (2005).
40. Oganov, A. R. & Ono, S. Theoretical and experimental evidence for a post-perovskite phase of $MgSiO_3$ in Earth's D" layer. *Nature* **430,** 445–448 (2004).
41. Sakai, T. *et al.* Fe–Mg partitioning between post-perovskite and ferropericlase in the lowermost mantle. *Phys. Chem. Miner.* **37,** 487–496 (2010).
42. Rohrbach, A. & Schmidt, M. W. Redox freezing and melting in the Earth's deep mantle resulting from carbon–iron redox coupling. *Nature* **472,** 209–212 (2011).
43. Stagno, V. *et al.* The stability of magnesite in the transition zone and the lower mantle as function of oxygen fugacity. *Geophys. Res. Lett.* **38,** L19309 (2011).
44. Frost, D. J. & McCammon, C. A. The redox state of Earth's mantle. *Annu. Rev. Earth Planet. Sci.* **36,** 389–420 (2008).
45. Liu, J., Lin, J.-F. & Prakapenka, V. B. High-pressure orthorhombic ferromagnesite as a potential deep-mantle carbon carrier. *Sci. Rep.* **5,** 7640, doi: 10.1038/srep07640 (2015).
46. Merlini, M. *et al.* The crystal structures of $Mg_2Fe_2C_4O_{13}$, with tetrahedrally coordinated carbon, and $Fe_{13}O_{19}$, synthesized at deep mantle conditions. *Am. Mineral.* **100,** 2001–2004 (2015).
47. Otsuka, K. & Karato, S. Deep penetration of molten iron into the mantle caused by a morphological instability. *Nature* **492,** 243–246 (2012).
48. Fei, Y. *et al.* Toward an internally consistent pressure scale. *Proc. Natl. Acad. Sci.* **104** (2007).
49. Suzuki, I. Thermal expansion of periclase and olivine, and their anharmonic properties. *J. Phys. Earth* **23,** 145–159 (1975).
50. Fei, Y., Mao, H.-K. & Hu, J. *P–V–T* equation of state of magnesiowüstite (Mg0.6Fe0.4)O. *Phys. Chem. Miner.* **18,** 416–422 (1992).
51. Dewaele, A., Datchi, F., Loubeyre, P. & Mezouar, M. High pressure-high temperature equations of state of neon and diamond. *Phys. Rev. B* **77,** 094106 (2008).

Acknowledgements

This work was supported by Grant-in-Aid awards for Scientific Research to E.O. (numbers 22000002 and 15H05748) from the Ministry of Education, Culture, Sports, Science, and Technology of Japanese Government. E.O. was also supported by Russian Science Foundation, Project 14B25.31.0032. The synchrotron radiation experiments were performed at SPring-8 with the approval of the Japan Synchrotron Radiation Research Institute (Proposal No. 2013B0104, 2014A0104, 2014B0104, 2015A0104, 2015B0104). F.M. was supported by the International Joint Graduate Program in Earth and Environmental Science (GP-EES), Tohoku Univirstiy.

Author Contributions

F.M., S.K., T.S., E.O., N.H. and Y.O. performed XRD measurements. F.M., S.K., E.O. and T.S. made arguments on geological applications of the experimental results and wrote the paper. All authors discussed the results and commented on the manuscript.

Additional Information

Supplementary information accompanies this paper at http://www.nature.com/srep

Competing financial interests: The authors declare no competing financial interests.

How to cite this article: Maeda, F. *et al.* Diamond formation in the deep lower mantle: a high-pressure reaction of $MgCO_3$ and SiO_2. *Sci. Rep.* **7**, 40602; doi: 10.1038/srep40602 (2017).

Publisher's note: Springer Nature remains neutral with regard to jurisdictional claims in published maps and institutional affiliations.